Phytomedicine 141 (2025) 156752

Contents lists available at ScienceDirect

Phytomedicine

journal homepage: www.elsevier.com/locate/phymed

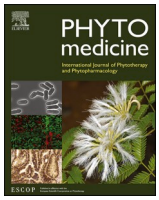

Original Article

Curcumol Ameliorates Cisplatin-induced Nephrotoxicity by Targeting TAK1 and Inhibiting MAPK and NF-κB Pathways

Xuejin Jin [a], Miao Yuan [a], Lingkun Wang [b], Huiyan Zha [b], Zhiwei Zheng [c], Zheng Xu [c], Jing Shi [a], Guang Liang [a], Qian Zhou [a,*]

[a] *School of Pharmaceutical Sciences, School of Food Science and Engineering, Hangzhou Medical College, Hangzhou, Zhejiang 311399, China*
[b] *Zhejiang Province Key Laboratory of Anti-Cancer Drug Research, Center for Drug Safety Evaluation and Research, College of Pharmaceutical Sciences, Zhejiang University, Hangzhou 310058, China*
[c] *Zhejiang Provincial People's Hospital, Affiliated People's Hospital, Hangzhou Medical College, Hangzhou 310014, China*

ARTICLE INFO

Keywords:
Acute kidney injury
Cisplatin
Curcumol
TAK1
MAPK
NF-Kb

ABSTRACT

Background: Although cisplatin (Cis) is a foundational chemotherapeutic agent, its dose-limiting nephrotoxicity lacks clinically effective drugs. *Curcumol* (CUR), a bioactive sesquiterpenoid derived from *Curcuma zedoariae* rhizome, exhibits multi-organ protective effects. However, its therapeutic potential and molecular targets in Cis-provoked acute kidney injury (AKI) remain unexplored.

Purpose: This study systematically investigated the nephroprotection and underlying mechanism of CUR in Cis-induced nephrotoxicity.

Methods: C57BL/6 mice received intraperitoneal administration of 20 mg/kg Cis to induce AKI. Dual-concentration CUR (40/80 mg/kg) was administered pre- and post-treatment in Cis-challenged mice, with longitudinal monitoring of renal function. Human tubular epithelial cells (HK-2 cells) were used to evaluate CUR's nephroprotection *in vitro*. RNA-sequencing transcriptomics identified pathway-level mechanisms, while structure-based molecular docking (MOD) prioritized target proteins.

Results: CUR exhibited dose-responsive nephroprotection, reducing apoptosis, oxidative stress, and inflammation more effectively than N-acetylcysteine in pre- and post-Cis treatment regimens. Mechanistically, we revealed that nephroprotection of CUR primarily involves suppression of phosphorylation-mediated MAPK/NF-κB pathway activation, thereby mitigating the inflammatory response. Notably, MOD and Cellular thermal shift assay (CETSA) data suggested a direct interaction between CUR and TAK1. Functional validation experiments demonstrated that *TAK1* silencing attenuated cisplatin-induced tubular cell injury, and TAK1 activity was essential for CUR's protective effects.

Conclusion: CUR ameliorated Cis-triggered AKI by targeting TAK1 and inhibiting MAPK and NF-κB pathways. These findings suggest that CUR may serve as a promising adjuvant to overcome the primary limitation of Cis.

Introduction

Acute kidney injury (AKI) represents a pervasive clinical entity and severe disorder distinguished by an unexpected deterioration in glomerular filtration rate and tubular reabsorption capacity over a short period, posing a considerable global public health challenge and participating in elevated morbidity and fatality (Kellum et al., 2021). Exposure to nephrotoxic chemicals remains a primary cause of AKI, with cisplatin (Cis), a highly potent treatment for various solid tumors, being constrained by its nephrotoxic effects in clinical use (Tang et al., 2023). Research has estimated that approximately 25 %–30 % of adult patients receiving Cis therapy develop AKI, and a substantial proportion of those who survive at least five years experience a persistent decline in their glomerular filtration capacity (Yu et al., 2023). Despite this, no

Abbreviations: AKI, Acute kidney injury; BCA, Bicinchoninic acid; BSA, Bovine serum albumin; BUN, Blood urea nitrogen; Cre, Serum creatinine; CCK-8, Cell counting kit-8; CETSA, Cellular thermal shift assay; Cis, Cisplatin; CUR, *Curcumol*; DAB, 3,3-Diaminobenzidine; DAPI, 4′,6-Diamidino-2-phenylindole; DEGs, Differentially expressed genes; ECL, Enhanced chemiluminescence; GSH-Px, Glutathione peroxidase; GO, Gene Ontology; H&E, Hematoxylin and eosin; HRP, Horseradish peroxidase; KEGG, Kyoto Encyclopedia of Genes and Genomes; KIM-1, Kidney injury molecule-1; MAPK, Mitogen-activated protein kinase.

* Corresponding author.
E-mail address: qianz1220@hmc.edu.cn (Q. Zhou).

https://doi.org/10.1016/j.phymed.2025.156752
Received 16 December 2024; Received in revised form 21 March 2025; Accepted 8 April 2025
Available online 9 April 2025
0944-7113/© 2025 Elsevier GmbH. All rights are reserved, including those for text and data mining, AI training, and similar technologies.

definitive and efficient clinical treatment exists for Cis-triggered AKI. Therefore, identifying an approach to mitigate the nephrotoxic effects of Cis has become an urgent priority that needs immediate attention and resolution.

In mouse models of AKI induced by high-dose Cis administration (20–30 mg/kg), primary pathological characteristics are tubular cell injury and necrosis, which are frequently exacerbated by inflammation (Tang et al., 2023). As a key driver of Cis-induced AKI, inflammation promotes immune cell infiltration, particularly macrophages, into the kidney tissue, affecting renal tubular epithelium and other resident kidney cells (Yao et al., 2022). At the lesion site, these cells, alongside pleiotropic soluble factors and metabolites, create a specialized micro-environment that derives disease progression (Wang et al., 2024). Stressed and damaged tubular cells further aggravate injury by releasing pro-inflammatory mediators, which either directly exacerbate tubular injury or recruit additional inflammatory cells (Song et al., 2024). Therefore, growing evidence supports anti-inflammatory strategies as a promising therapeutic approach for AKI.

Natural products have recently garnered increasing attention for their potential in preventing and managing kidney diseases (Fang et al., 2021; Gao et al., 2023). *Curcumol* (CUR, Fig. 1A), a monomer extracted from *Curcuma zedoariae*, exhibits potent anti-inflammatory properties across various diseases (Li et al., 2020; Nie et al., 2023; Wei et al., 2019). For example, CUR inhibits Wnt/β-catenin signaling, alleviating lung inflammation in chronic asthmatic murine models (Jia et al., 2021). It also protects the heart by suppressing inflammation and programmed cell death by governing AKT/NF-κB signaling (Shao et al., 2023). Additionally, CUR administration mitigates brain injury and neuro-inflammation by modulating the anti-inflammatory polarization of microglia (Liu et al., 2024). Despite these established effects, the role

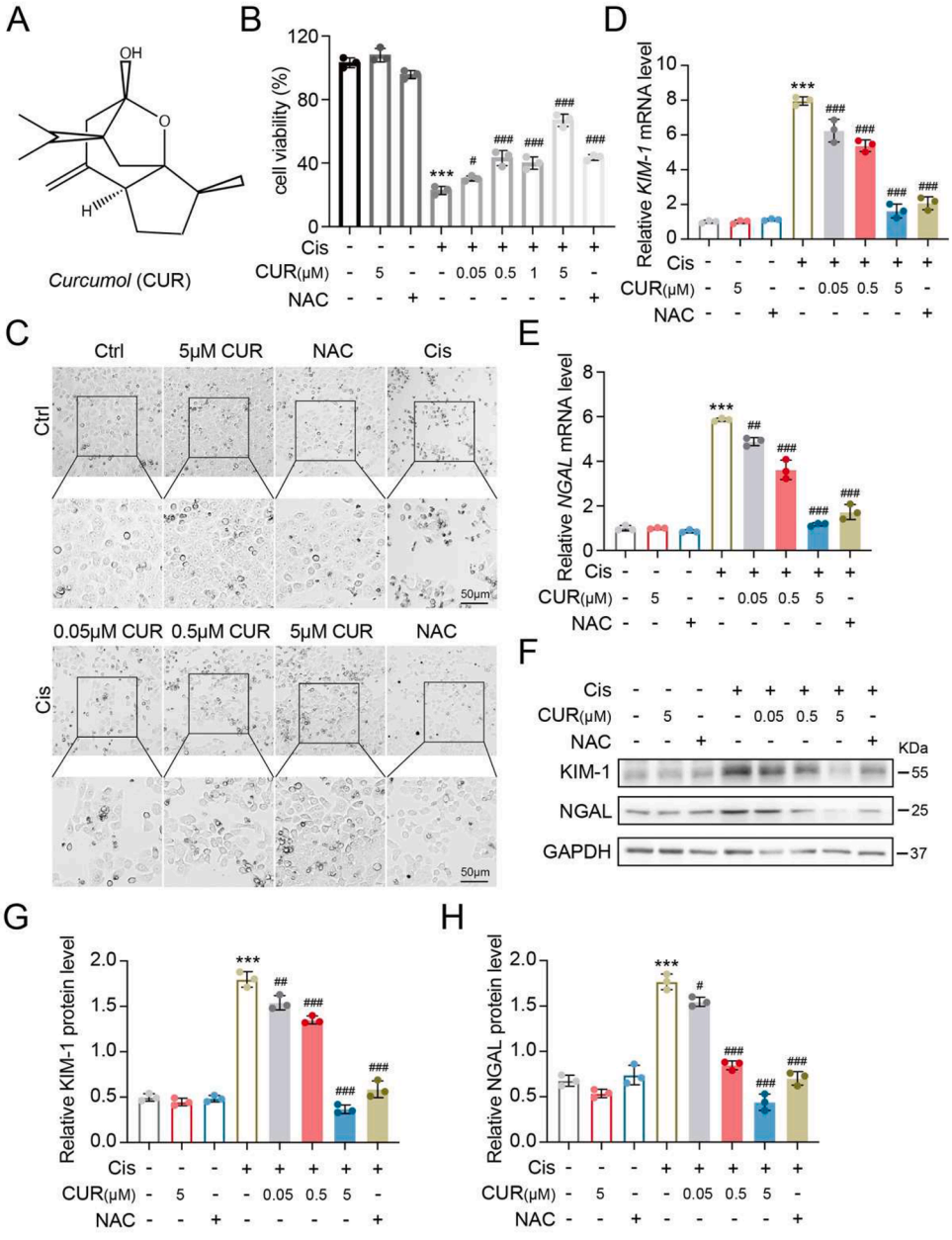

Fig. 1. CUR alleviated Cis-induced kidney injury in HK-2 cells. (A) CUR chemical structure. (B) Effect of CUR (0.05–5 μM) and 1 mM NAC on HK-2 cell viability treated with 5 μM Cis. (C) Bright-field microscope images of HK-2 cell morphology. Scale bar = 50 μm. (D-E) RT-qPCR: mRNA expression levels of *KIM-1* and *NGAL* in HK-2 cells; normalized to *Gapdh*. (F) Representative Western blotting analysis: KIM-1 and NGAL protein levels in HK-2 cells; GAPDH as the loading control. (G-H) Quantitative analysis: KIM-1 and NGAL protein levels. $n = 3$ independent experiments.

and underlying mechanism in Cis-associated nephrotoxicity remains unexplored.

This study demonstrated that CUR treatment exhibits significant nephroprotective efficacy against Cis-associated renal tubular injury in both HK-2 cells and C57BL/6 murine models. An analysis utilizing RNA-sequencing (RNA-seq) unveiled that CUR suppresses the expression levels of inflammatory response-associated genes, primarily by mediating MAPK and NF-κB signaling in Cis-induced AKI. MOD and CETSA analyses further suggested that CUR might direct target TAK1, inhibiting phosphorylation and inactivating MAPK and NF-κB pathways. These findings highlight CUR as a probable therapeutic approach for mitigating Cis-triggered AKI.

Materials and methods

Reagents

CUR (99.87 % purity), extracted from the rhizome of *C. zedoariae*, was sourced from the National Institutes for Food and Drug Control, Beijing, China while obtaining Cis (99.63 % purity, T1564) from TargetMol, Shanghai, China.

Cell culture

Human renal proximal tubular cells (HK-2, CRL-2190, ATCC) were cultured in RPMI-1640 medium (BC-M-017, Bio channel, Nanjing, China), that contained 10 % fetal bovine serum (BS-1102, OPCEL, Hohhot, China) and 1 % penicillin-streptomycin (BC—CE-007 Bio channel, Nanjing, China) at 37 °C with a humidified conditions comprising 5 % CO_2.

Cell counting kit-8 (CCK-8) assay

CUR cytotoxicity was assessed in HK-2 cells through a CCK-8 kit (K1018, APExBIO, HOU, USA) by plating the cells into 96-well culture plates (3×10^3 cells/well), and treated for 24 h with diverse concentrations (0, 0.05, 0.5, 1, and 5 μM). Then, 100 μl of serum-containing media supplemented with 10 % (v/v) CCK-8 reagent was introduced to each well and incubated for 2 h at 37 °C, therefore quantifying absorbance at 450 nm using a microplate reader (Thermo Fisher Scientific, Multiskan FC, USA).

Animal experiments

Male C57BL/6 mice (6–8 weeks, SPF facility at Hangzhou Medical College's Laboratory Animal Center) were housed under a 12-h dark and light cycle at 24 ± 2 °C and humidified conditions of 55 % ± 5 % and a normal diet with free food and water access. The Institutional Animal Care and Use Committee of Hangzhou Medical College authorized the experimental protocols and animal care (Registration Number: 2024–169, ethical approval date: 6/20/2024).

For evaluating the CUR preventive effect on Cis-induced AKI, mice were equally allocated at random into seven groups ($n = 7$): Control (Ctrl), Cis (20 mg/kg), CUR (80 mg/kg), N-acetylcysteine (NAC, 100 mg/kg), CUR (40 mg/kg) + Cis, CUR (80mg/kg) + Cis, and NAC (100 mg/kg) + Cis groups. CUR or NAC was administered using gavage for 5 consecutive days. On day 3, 20 mg/kg Cis was injected intraperitoneally as a single dose.

For assessing the therapeutic effect of CUR on Cis-induced AKI, the mice were equally separated at random into seven groups ($n = 7$): Ctrl, Cis (20 mg/kg), CUR (80 mg/kg), NAC (100 mg/kg), Cis + 40 mg/kg CUR, Cis + 80 mg/kg CUR, and Cis + 100 mg/kg NAC. Cis (20 mg/kg) was injected intraperitoneally. CUR or NAC was administered using gavage 2 h later and consecutive for 3 days.

Eventually, the animals were anesthetized and sacrificed using an intraperitoneal injection of a 0.3 % pentobarbital sodium solution (10 ml/kg). Renal tissue samples were rapidly frozen in liquid nitrogen for subsequent molecular analyses, or alternatively, they were fixed using 4 % PFA for histopathological examination.

Serum biochemical measurement

Blood samples were obtained for biochemical assessment. Centrifugation was conducted for 15 min at 4 °C at 2000 rpm to produce the serum. Blood urea nitrogen (BUN) and creatinine (Cre) were measured using an automatic blood biochemical analyzer (Roche, Cobas c311, Switzerland).

Renal histopathology

The H&E staining was utilized to assess the renal damage score after fixing the kidney tissues of mice with 4 % PFA, dehydrating, paraffin-embedding, and sectioning into 4 μm thick slices. The histopathology examination found cast development, necrosis, and renal tubular injury. The renal tubular injury was assessed using the afflicted tubule proportion: 0 (no injury), 1 (<25 %), 2 (25 %–50 %), 3 (50 %–75 %), and 4 (>75 %).

Immunohistochemical determination

Paraffin-embedded renal tissue sections were sequentially processed through xylene-mediated deparaffinization and rehydration. Endogenous peroxidase activity was quenched by 3 % hydrogen peroxide (v/v) for 15 min at RT, thereby blocking non-specific binding sites with 5 % bovine serum albumin (BSA, BS114–100 g, Biosharp, Hefei, China). Tissue sections were incubated with anti-F4/80 primary antibody (1:200, DF2789, Affinity, Jiangsu, China) for a whole night at 4 °C. Positive reactions were detected *via* horseradish peroxidase-conjugated secondary antibodies. Immunoreactivity was visualized with 3,3'-diaminobenzidine (Beyotime, China). Tissue sections were subjected to counterstaining with hematoxylin and dehydrating, examined by a Nilon Eclipse E200 light microscope, digitally captured, and analyzed using ImageJ software.

RNA extraction, qPCR, and RNA-seq

RNAex reagent (AG21101) and an RNA extraction kit (AG21024) were utilized for total RNA isolation, then reversely transcripted the extracted RNA to cDNA using Evo M-MLV reverse transcription premixed type kit (AG11728). A 10 μl reaction mixture containing the SYBR Green Pro Taq HS premixed kit (AG11733, all from AG, Hunan, China) was employed to conduct real-time qPCR (RT-qPCR). CFX Connect Real-Time PCR Detection System (BIO-RAD, *CA*, USA) was employed to conduct the PCR analysis. Gene expression was measured through the $2^{-\Delta\Delta CT}$ method, with data normalized to *Gapdh*. Table 1 lists the primer sequences used for qPCR. A portion of the kidney tissue was utilized for RNA-seq.

Western blotting analysis

Renal cortical tissues underwent extraction to obtain total proteins, utilizing RIPA buffer added with protease and phosphatase inhibitors. The quantity of proteins was determined using a bicinchoninic acid-based protein kit (P0006, Beyotime, Shanghai, China). The extracted proteins were separated *via* 10 % SDS-PAGE gel electrophoresis and transferred onto 0.45 μM PVDF membrane (C3117, Millipore, MA, USA). After a 1-hour blocking period at RT using 5 % skim milk powder, the PVDF membranes were washed and incubated with the primary antibody at 4 °C overnight. The specific primary antibodies utilized in the experiments included: KIM-1 (1:2000, ab47635, Abcam), NGAL (1:1000, DF6816, Affinity), c-PARP (1:1000, ET1608–10, HUABIO), Bcl2 (1:1000, AF6139, Affinity), Bax (1:1000, 50,599–2-Ig,

Table 1
Primer sequences.

Gene	Primer sequences (5'–3')
mKIM-1	F: *AGTGTGACGTTGACATCCGT* R: *GTAACAGTCCGCCTAGAAGC*
mNGAL	F: *TGAGTGTCATGTGTCTGGGC* R: *AACTGATCGCTCCGGAAGTC*
mTnfα	F: *CCCTCACACTCACAAACCAC* R: *ATAGCAAATCGGCTGACGGT*
mIl6	F: *ACAAAGCCAGAGTCCTTCAGAG* R: *GTGACTCCAGCTTATCTCTTGGT*
mIl1b	F: *GCCACCTTTTGACAGTGATGAG* R: *GACAGCCCAGGTCAAAGGTT*
mBax	F: *GACACTGGACTTCCTCCGTG* R: *ATGTGGGGGTCCCGAAGTAG*
mBcl2	F: *AGTACCTGAACCGGCATCTG* R: *CTTGTGGCCCAGGTATGCAC*
mGapdh	F: *GCCTCCTCCAATTCAACCCTT* R: *CCAAATCCGTTCACACCGAC*
hKIM-1	F: *AAGTTCTTCCGTGGCCCTTT* R: *ATCAGCGTTCAGATCCAGGC*
hNGAL	F: *TGAGTGCACAGGTGCCG* R: *TTTAGCAGACAAGGTGGGGC*
hTnfα	F: *GACAAGCCTGTAGCCCATGT* R: *GGAGGTTGACCTTGGTCTGG*
hIl6	F: *TTCGGTCCAGTTGCCTTCTC* R: *TCTTCTCCTGGGGGTACTGG*
hIl1b	F: *CAGAAGTACCTGAGCTCGCC* R: *GAAGCCCTTGCTGTAGTGGT*
hBax	F: *CCCAGAGGCGGGGTTTCAT* R: *AGCTGCCACTCGGAAAAAGA*
hBcl2	F: *TCAACATCTTCCCTGGGCAC* R: *GGGAGCCTGATGGTGAACTC*

Proteintech), ERK (1:2000, #9102), p-ERK(1:2000, #9101, both from Cell Signaling Technology), JNK (1:2000, sc-571), p-JNK (1:2000, sc-81,502, both from Santa), P38 (1:1000, #9212, Cell Signaling Technology), p-P38 (1:1000, AF4001, Affinity), IκBα (1:2000, 10,268–1-AP, Proteintech), p-IκBα (1:2000, AF2002, Affinity), p65 (1:2000, 10,745–1-AP, Proteintech), p-p65 (1:1000, AF2006), TAK1 (1:2000, AF7616), p-TAK1 (1:1000, AF3019, all from Affinity), β-actin(1:5000, K101527P, Solarbio), and GAPDH (1:10,000, #2118, Cell Signaling Technology). HRP-conjugated secondary antibodies were applied for 1 h at RT. Subsequently, the visualization of protein bands was conducted *via* an improved chemiluminescence kit and quantification was carried out with ImageJ software. GAPDH or β-actin served as the normal control.

TUNEL assay

TUNEL Apoptosis Assay Kit (C1086, Beyotime, Shanghai, China) was employed to assess cell apoptosis, and we captured images *via* a fluorescence microscope (EVOS M7000, Invitrogen, *CA*, USA).

Reactive oxygen species (ROS) assay

HK-2 cells were subjected to Cis (5 μM) and CUR (50 nM, 500 nM, and 5 μM) for 24 h, and ROS levels were measured by the ROS Assay Kit (S0033S, Beyotime, Shanghai, China) following the manufacturer's instructions.

Glutathione peroxidase (GSH-Px) and total superoxide dismutase (SOD) assays

The levels of oxidative stress in both HK-2 cells and kidney tissues were evaluated by measuring GSH-Px and total SOD levels using commercially available kits (Beyotime, Shanghai, China).

ELISA for cytokine assays

Supernatants from serum and cell culture were analyzed for tumor necrosis factor (TNF)-α (E-EL-M3063), interleukin (IL)-6 (E-EL-M0044), and IL-1β (E-EL-M0037) *via* ELISA kits (Elabscience) as *per* the manufacturer's guidelines.

Molecular docking

The crystal structures of human TAK1 (Protein Data Bank (PDB) code: 5JGD) were obtained from the PDB database. CUR chemical structure was retrieved from PubChem and processed using OpenBabel software (v2.4.1). MOD was carried out using AutoDock software (v4.2.6) following the protocols, analyzing the binding energy to predict potential interactions. The results were visualized using Pymol and Schrodinger Maestro software.

Kinase activity assay

The enzymatic activities including ERK, JNK, P38, and IKKα assays were performed by PreceDo Pharmaceuticals Co. Ltd. (Hefei, China).

Cellular thermal shift assay (CESTA)

HK-2 cell were lysed using liquid nitrogen of freeze-thaw cycles. The cell lysates were incubated with either CUR (5 μM) or DMSO at RT for 60 min. And then the samples treated with CUR or DMSO were heated at 41 °C, 44 °C, 47 °C, 50 °C, 53 °C, 56 °C, 59 °C, and 62 °C for three minutes. The supernatants were harvested and subjected to Western blotting to assess TAK1 protein expression levels.

TAK1 silencing

The synthesis of small interfering RNA (siRNA) targeting human *TAK1* was conducted by KeyGEN Co.Ltd. (Nanjing, China) with the following sequences: sense: *GGUAGUAAUUACAGUGAAATT*, and antisense: *UUUCACUGUAAUUACUACCTT*. A scrambled siRNA served as the negative control during the transfection process. A final concentration of 50 nM siRNA was combined with 4 μl of jetPRIME® transfection reagent (101,000,046, Polyplus, Illkirch, France) in 200 μl of jetPRIME® buffer, and the mixture was incubated at RT for 10 min. Following the incubation, the mixture was introduced to the HK-2 cells. Knockdown efficiency was confirmed by Western blotting analysis.

NF-κB (P65) staining

The NF-κB (P65) translocation analysis required first fixing the HK-2 cells with 4 % PFA for 20 min and then permeabilized them with 0.1 % Triton X-100 for 10 min. Then, cells were blocked with 1 % BSA in phosphate-buffered saline for a period of 1 h, followed by incubation at 4 °C for a whole night with anti-NF-κB (p65) antibody (1:200, 10,745–1-AP, Proteintech). Afterward, a 1-h incubation of the cells was conducted with fluorescent-labeled secondary antibodies in the darkness at RT. The nuclei were then stained to DAPI stain for 5 min in the darkness at RT. Staining was visualized using a fluorescence microscope.

Statistical analysis

Data were analyzed with GraphPad Prism (v9.5.1) and ImageJ (v1.8.0) and expressed as means ± standard deviation (SD). One-way ANOVA followed by Tukey's *post-hoc* test was utilized to detect statistical significance. $p < 0.05$ indicated statistical significance. $^{*}p < 0.05$, ** $p < 0.01$, *** $p < 0.001$ vs. Ctrl; $^{\#}$ $p < 0.05$, $^{\#\#}$ $p < 0.01$, $^{\#\#\#}$ $p < 0.001$ vs. Cis group.

Results

CUR alleviates cis-induced injury in HK-2 cells

As proximal renal tubular epithelium is the primary target of Cis-induced nephrotoxicity, leading to AKI, HK-2 cells were selected to determine the capability of CUR in mitigating Cis-provoked nephrotoxicity *in vitro*. The impact of various CUR concentrations (0.05, 0.5, 1, and 5 μM) on Cis-treated HK-2 cells was evaluated, with NAC serving as a positive control, as it has been reported to protect HK-2 cells from Cis-triggered injury (Fang et al.; 2021). The CCK-8 assay revealed that CUR reduced Cis-triggered cell death in a concentration-dependent manner, with 5 μM CUR providing greater protection than NAC without inducing cytotoxicity (Fig. 1B). Protective properties of CUR were analyzed at concentrations of 0.05, 0.5, and 5 μM. Bright-field micrographs of HK-2 cells demonstrated that CUR notably decreased Cis-induced cell damage, indicating its effect on restoring the health of nephron cellular membranes (Fig. 1C). The messenger RNA (mRNA) levels of the renal tubular damage key markers: *KIM-1* and *NGAL,* were significantly upregulated in HK-2 cells exposed to Cis, which were significantly mitigated by CUR therapy (Fig. 1D-E). Similarly, KIM-1 and NGAL protein levels were reduced following CUR administration in Cis-stimulated HK-2 cells (Fig. 1F–H). Collectively, CUR provides protective effects against Cis-provoked nephrotoxicity *in vitro*.

CUR attenuates cis-provoked apoptosis, oxidative stress, and inflammation in HK-2 cells

Apoptosis, oxidative stress, and inflammation are crucial in Cis-induced AKI. The effects of CUR on these pathological factors were investigated. DAPI staining of HK-2 cell nuclei revealed that CUR markedly reversed Cis-induced apoptotic changes, including cellular condensation and nuclear fragmentation (Fig. 2A). TUNEL staining further confirmed that CUR lowered Cis-provoked HK-2 cell apoptosis (Fig. 2B). Western blotting and RT-qPCR results demonstrated that CUR significantly suppressed the enhanced c-PARP and Bax expression, and increased the reduced Bcl2 triggered by Cis in HK-2 cells (Fig. 2C and S1A–D). Elevated levels of intracellular ROS are known to cause cell damage. Total SOD and GSH-Px activities were evaluated to assess oxidative stress, revealing that CUR restored the activities of these antioxidants, which were impaired by Cis (Fig. 2D-E). 2′,7′-Dichlorodihydrofluorescein diacetate (DCFH-DA) probe staining demonstrated that CUR treatment notably decreased the count of positive cells in Cis-treated HK-2 cells (Fig. 2F). ELISA and RT-qPCR results indicated that CUR downregulated TNF-α, IL-6, and IL-1β in Cis-induced cells (Fig. 2G–I and S1E–G). These findings suggest that CUR suppresses cell apoptosis, oxidative stress, and inflammation in Cis-induced nephrotoxicity.

CUR pre-treatment protects against cis-induced AKI in mice

CUR (40 and 80 mg/kg) or NAC (100 mg/kg) was administered

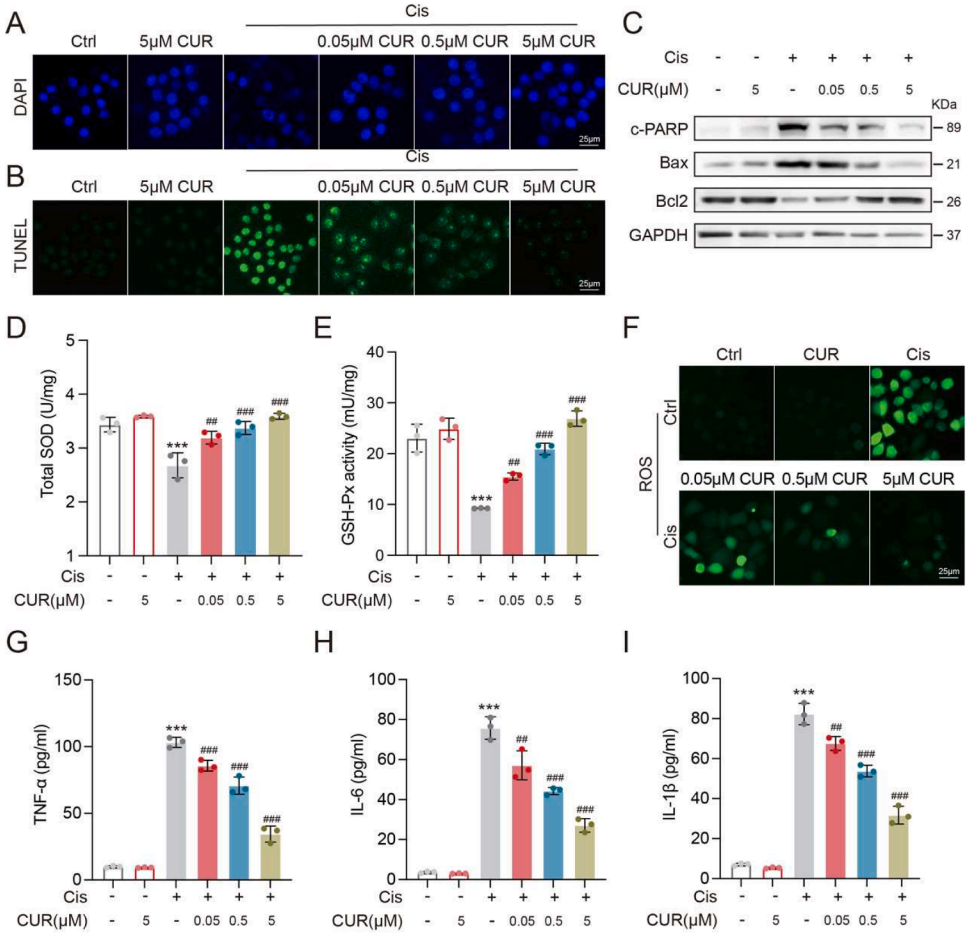

Fig. 2. CUR reduced Cis-provoked apoptosis, oxidative stress, and inflammation in HK-2 cells. (A) DAPI and (B) TUNEL staining images. Scale bar = 25 μm. (C) Western blotting analysis: c-PARP, Bax, and Bcl2 protein levels in HK-2 cells; GAPDH as the loading control. (D) Total SOD levels and (E) GSH-Px activity in HK-2 cells. (F) ROS staining images. Scale bar = 25 μm. (G–I) ELISA: TNF-α, IL-6, and IL-1β levels in HK-2 cell supernatant. $n = 3$ independent experiments.

intragastrically for five successive days, with a single intraperitoneal administration of 20 mg/kg Cis on day 3 to explore its preventive effect on Cis-provoked AKI in a murine model (Fig. 3A). Serum and renal tissue samples were collected on day 6. Biochemical analysis revealed severe nephrotoxicity in Cis-treated mice, as indicated by significantly elevated serum BUN and Cre levels. However, CUR or NAC treatment effectively reduced these elevated levels (Fig. 3B-C). Kidneys in the Cis group pronounced white discoloration and edema, whereas CUR or NAC administration improved their appearance (Fig. 3D). H&E staining of kidney tissues revealed that Cis-induced renal tubular injury was marked by tubular dilatation, tubular cell necrosis, brush border loss, tubular vacuolization, and tubular protein cast formation. Notably, CUR (80 mg/kg) administration significantly alleviated these histopathological abnormalities, demonstrating a more substantial preventive effect than NAC (100 mg/kg) (Fig. 3E-F). Additionally, CUR reduced the mRNA levels (Fig. 3G-H) and protein expression levels (Fig. 3I–l) of KIM-1 and NGAL. Apoptotic changes and inflammatory cytokines were also investigated in kidney tissues, indicating that CUR pre-treatment could reduce cell apoptosis (Fig. S2A–D) and inflammation (Fig. S2E–G). Pre-treatment of CUR was performed *in vitro* to align with the *in vivo* effect. Bright-field micrographs of HK-2 cells revealed that CUR prevented Cis-mediated cell damage (Fig. S2H). CUR pre-treatment inhibited *KIM-1* and *NGAL* mRNA levels (Fig. S2I-J). These findings imply that CUR possesses the capability to prevent Cis-induced AKI.

CUR post-treatment mitigates cis-provoked AKI in mice

To further ascertain the therapeutic capability of CUR in Cis-triggered AKI, mice received 40 and 80 mg/kg of CUR or 100 mg/kg of NAC using gavage at 2, 24, and 48 h following Cis treatment (Fig. 4A). Serum and renal tissue samples were collected on day 4. As anticipated, CUR and NAC therapy significantly diminished serum BUN and Cre

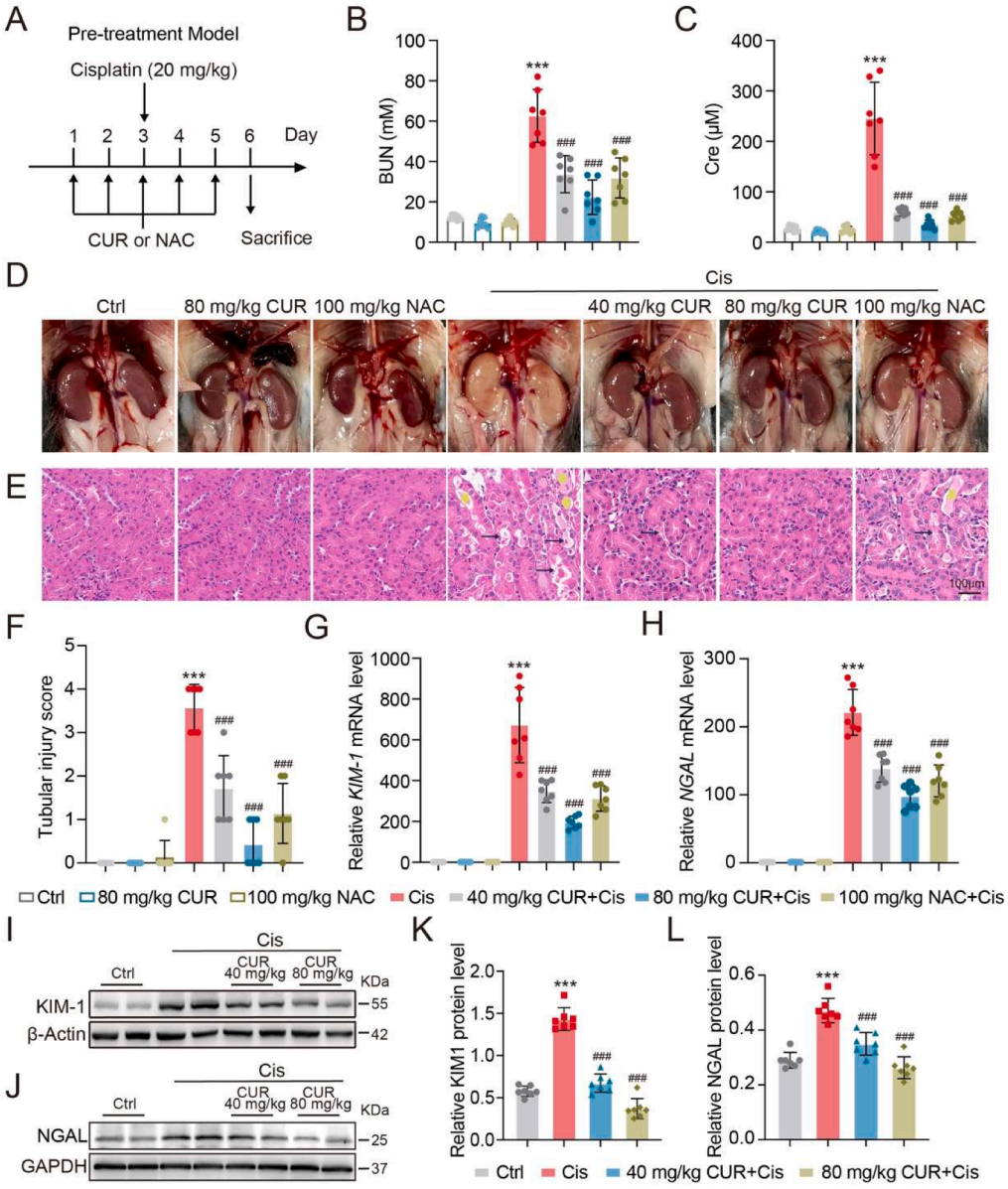

Fig. 3. CUR protected against Cis-induced nephrotoxicity in mice. (A) An illustration of CUR or NAC administration for preventing Cis-induced AKI. (B-C) Serum BUN and Cre levels after 72 h of Cis-injection. (D) Images of renal morphology in each group. (E) H&E-stained images. Arrows indicate tubular dilatation and necrosis, while asterisks denote cast formation. Scale bar = 100 μm. (F) Tubular injury score analysis. (G-H) RT-qPCR analysis of *KIM-1* and *NGAL* mRNA levels in mouse renal tissues and data normalized to *Gapdh*. (I-J) Representative Western blotting analysis of KIM-1 and NGAL protein levels in mouse renal tissues, with β-actin or GAPDH as the loading control. (K-l) Quantification analysis: KIM-1 and NGAL protein levels. $n = 7$ animals *per* group.

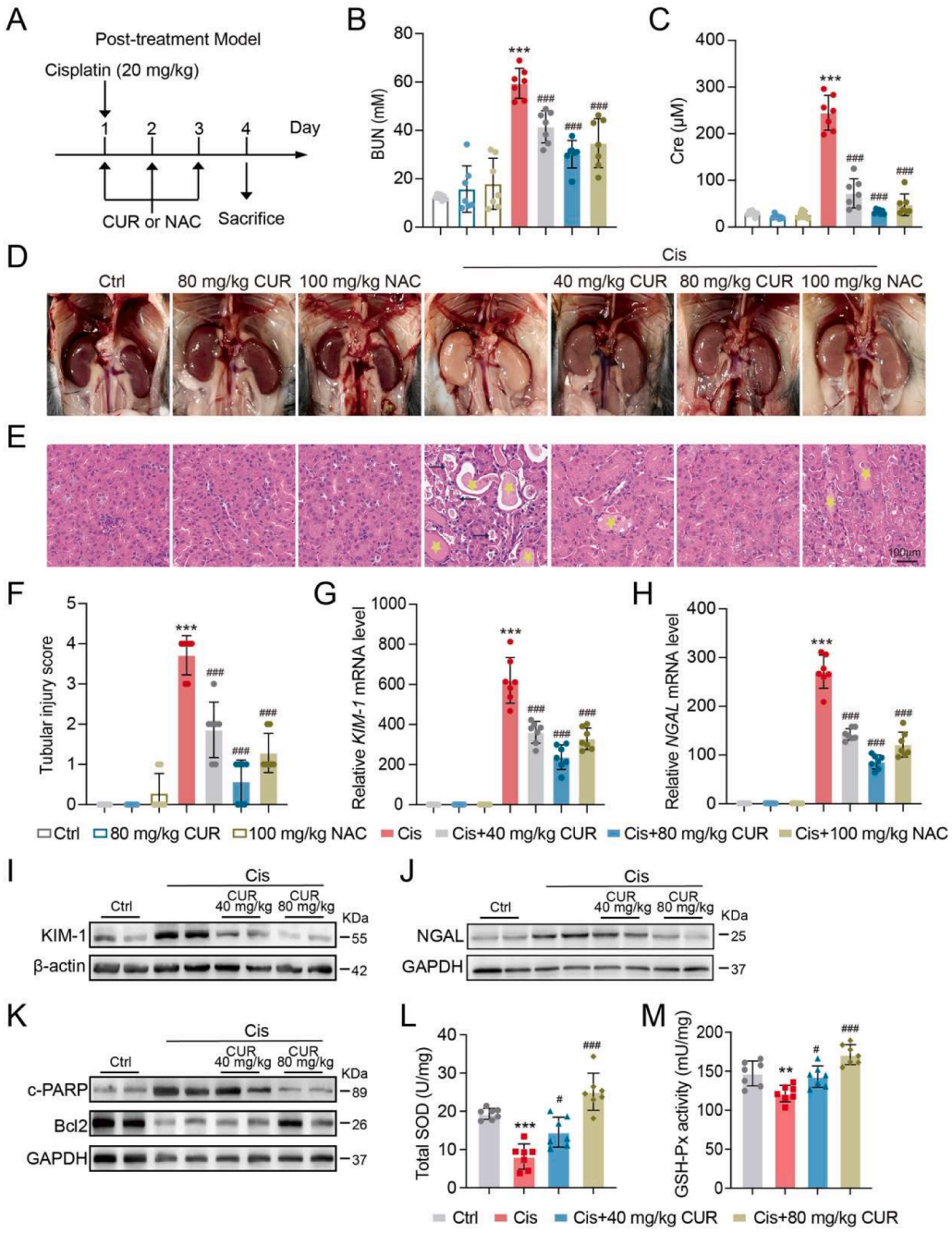

Fig. 4. CUR mitigated Cis-provoked AKI in mice. (A) Systematic illustration of CUR or NAC treatment to attenuate Cis-triggered AKI. (B-C) The levels of serum BUN and Cre following 72 h Cis injection. (D) Representative images of kidney morphology in each group. (E) Representative H&E images, where arrows indicate tubular dilatation and necrosis, and asterisks denote cast formation. Scale bar = 100 μm. (F) Tubular injury score analysis. (G-H) RT-qPCR: *KIM-1* and *NGAL* mRNA levels in mouse renal tissues; normalized to *Gapdh*. (I–K) Western blotting: KIM-1, NGAL, c-PARP, and Bcl2 protein levels; β-actin or GAPDH as the loading control. (l) Total SOD levels in mouse renal tissues. (M) GSH-Px activity in mouse renal tissues. $n = 7$ animals *per* group.

levels in Cis-triggered AKI mice (Fig. 4B-C). Besides, the morphology of the kidneys indicated a substantial improvement in the blood supply following CUR treatment (Fig. 4D). H&E staining confirmed that CUR alleviated tubular necrosis and degeneration in Cis-induced AKI mice, indicating a superior efficacy than NAC (Fig. 4E-F). RT-qPCR and Western blotting results revealed significantly reduced KIM-1 and NGAL levels following CUR treatment (Fig. 4G–J and S3A-B). Furthermore, CUR mitigated cell apoptosis in mouse renal tissues by downregulating c-PARP and Bax while upregulating Bcl-2 (Fig. 4K and S3C–F). Moreover, CUR restored total SOD and GSH-Px activities which were impaired by Cis (Fig. 4l-M). Importantly, no obvious organ injury, including heart, liver, spleen, and lung, was observed after CUR (80mg/kg) administration, unlike the Ctrl (Fig. S3G). Collectively, CUR is a promising therapeutic candidate for Cis-provoked AKI in clinical practice.

CUR inhibits inflammatory response and macrophage infiltration in vivo

Kidney tissues were collected from mice treated with either Cis alone or combined with CUR. RNA-seq was performed on these tissues to cover the mechanism behind CUR's therapeutic effect on Cis-triggered AKI in mice. Gene ontology (GO) results showcased that differentially

expressed genes (DEGs) were primarily associated with acute inflammatory response, oxidative stress, and apoptotic signaling pathways (Fig. 5A). A heatmap of inflammatory response-related genes demonstrated that CUR inhibited Cis-induced pro-inflammatory factors (Fig. 5B). RT-qPCR was performed on mouse tissues to validate the heatmap findings (Fig. 5C). Macrophages play crucial roles in AKI and are closely linked to renal inflammation (Privratsky et al., 2023; Tang et al., 2019; Yao et al., 2022). Immunohistochemical staining using a macrophage-specific antibody (F4/80) revealed increased F4/80$^+$ macrophages in the Cis group, while CUR treatment reduced their infiltration in renal tissues (Fig. 5D-5E). To further determine whether other immune cells were involved, immunohistochemical staining was performed for dendritic cells (CD11C$^+$), neutrophils (MPO$^+$), T cells (CD4$^+$), and B cells (CD19$^+$). There was no significant difference between the Cis and CUR groups (Fig. S4A–D). Additionally, ELISA and RT-qPCR analyses were performed in serum and mouse renal tissues to assess TNF-α, IL-6, and IL-1β levels. Cis notably enhanced the inflammatory response, while CUR treatment markedly reduced TNF-α, IL-6, and IL-1β levels (Fig. 5F–H and S4E–G). These results indicate that CUR alleviates the renal inflammatory response primarily driven by macrophages in Cis-induced AKI mice.

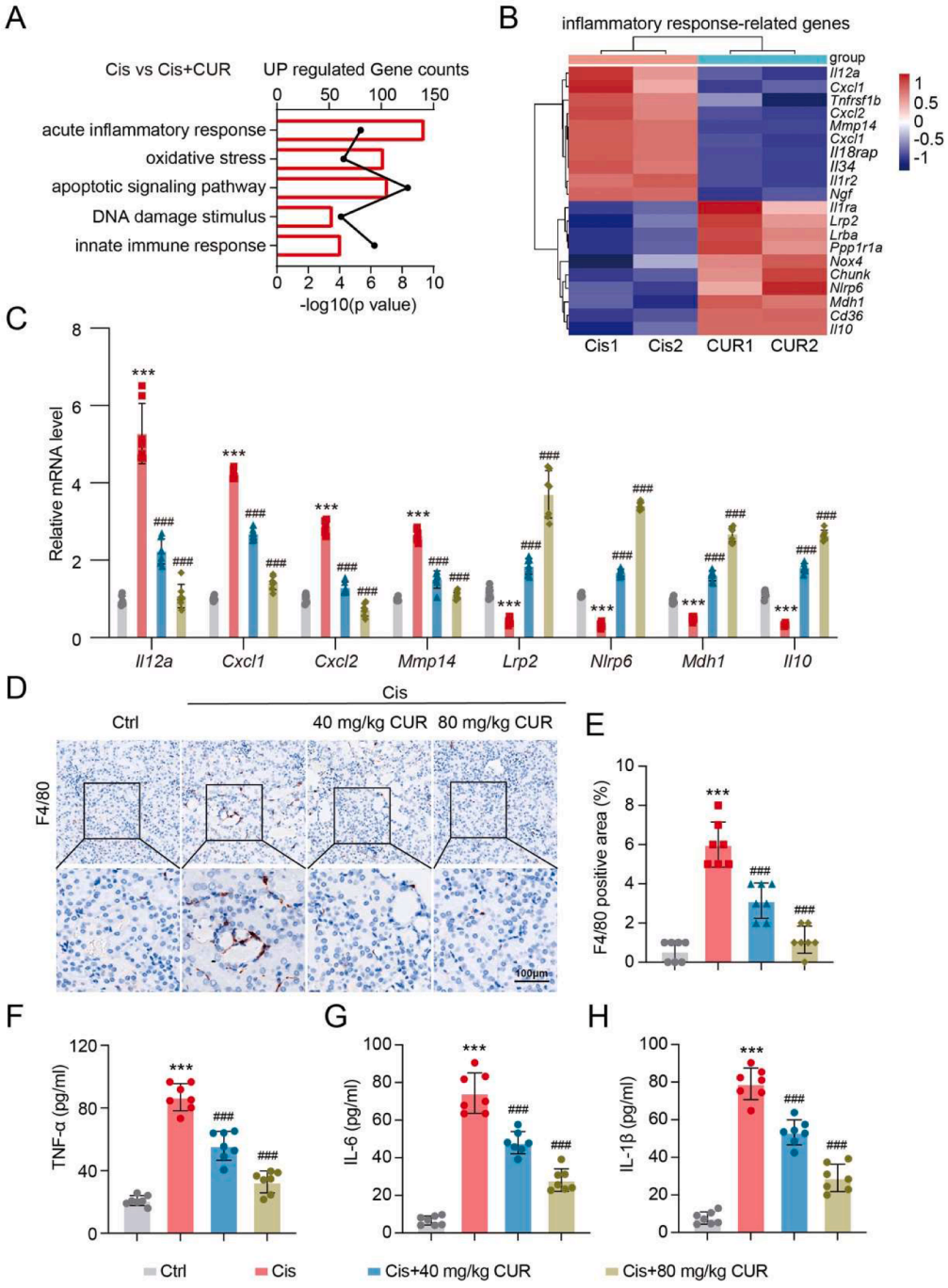

Fig. 5. CUR treatment mitigated the inflammatory response and macrophage infiltration in mice. (A) GO analysis of upregulated gene enrichment in Cis-treated mice with or without CUR. (B) Heatmap: DEGs associated with the inflammatory response. (C) RT-qPCR: *Il12a, Cxcl1, Cxcl2, Mmp14, Lrp2, Nlrp6, Mdh1, and Il10* mRNA levels in kidney tissues; data normalized to *Gapdh*. (D) Representative immunohistochemical staining images for F4/80$^+$ macrophages. Scale bar = 100 μm. (E) Quantitative analysis of F4/80$^+$ macrophages. (F–H) ELISA: TNF-α, IL-6, and IL-1β levels presented in Fig. 4A mouse model. $n = 7$ animals *per* group.

CUR protected mice against cis-induced AKI and lowered the inflammatory response by impeding MAPK and nf-κb signalings

RNA-Seq analysis was applied to uncover the signaling behind the CUR-mediated suppression of inflammatory response. The volcano plot indicates 7032 significant DEGs, with 3732 upregulated genes and 3300 downregulated genes in the Cis group relative to the Ctrl. A comparison between Cis and CUR groups identified 3630 DEGs, including 1496 upregulated and 2134 downregulated genes (Fig. 6A-B). The Venn diagram illustrates that 1069 genes were overexpressed in the Cis group but downregulated following CUR treatment (Fig. 6C). The outcomes of KEGG enrichment analysis pinpointed MAPK and NF-κB signalings as key contributors to the inflammatory response (Fig. 6D). Western blotting assays demonstrated a significant upregulation of MAPK pathway components, including p-ERK, p-JNK, and p-P38, in Cis-treated mouse kidney tissues. In contrast, CUR effectively suppressed the MAPK pathway activation *in vivo* and *in vitro* (Fig. 6E-F and S5A-B). Simultaneously, CUR treatment inhibited NF-κB pathway activation, as evidenced by p-p65 and p-IκBα degradation in mouse kidney tissues and HK-2 cells (Fig. 6G-H and S5C-D). Additionally, enzymatic activity assays revealed that CUR reduced the activities of ERK1/2, JNK1/2, P38, and IKKα *in vitro* (Fig. S5E). These findings suggest that CUR attenuates Cis-induced AKI by hampering MAPK and NF-κB signalings.

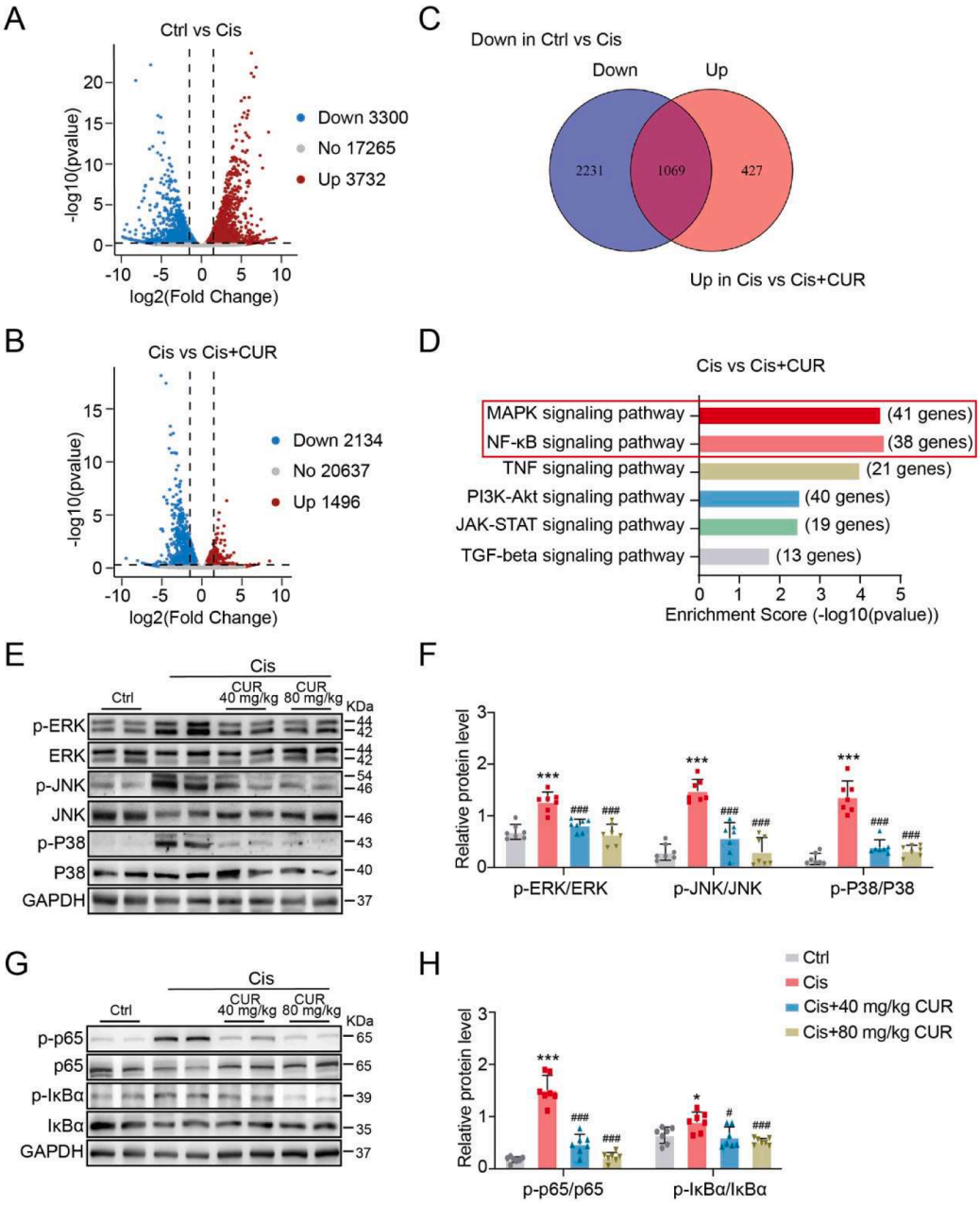

Fig. 6. CUR alleviated Cis-provoked AKI in mice by impeding MAPK and NF-κB pathways. (A-B) Volcano plots: DEGs in the comparison between Ctrl and Cis groups and between Cis and Cis + CUR groups, respectively. (C) Venn diagram: Number of genes regulated by Cis alone or combined with CUR. (D) KEGG enrichment analysis: Upregulated genes in Cis-treated mice with or without CUR. (E-F) The protein levels of ERK, JNK, P38, p-ERK, p-JNK, and p-P38 were detected by Western blotting and quantified using ImageJ software; GAPDH as the loading control. (G-H) The protein expression levels of p65, IκBα, p-p65, and p-IκBα were analyzed by Western blotting and quantified *via* ImageJ software, with GAPDH as the loading control. $n = 7$ animals *per* group.

CUR attenuates cis-induced AKI by inhibiting TAK1

To further investigate the mechanism through which CUR suppresses the MAPK and NF-κB pathways, TAK1 was examined as a crucial upstream regulatory kinase essential for both signaling pathways and inflammatory responses (Wang et al., 2022). Mice with TAK1 deletion in their proximal tubules exhibited reduced kidney dysfunction, tubular injury, and apoptosis following Cis-induced AKI (Zhou et al., 2020). MOD evaluated the affinity of CUR with TAK1, indicating a potential bonding interaction (affinity = –5.73 ± 0.12 kcal/mol, pKi = 4.21 ± 0.09 μM) (Fig. 7A). CETSA revealed that the decline in TAK1 protein levels slowed down when incubated with CUR compared to DMSO (Fig. S6A-B). Enzymatic activity assays validated that CUR reduced the activities of TAK1 (Fig. S6C). CUR treatment markedly suppressed the TAK1 phosphorylation, which was induced by Cis in kidney tissues (Fig. 7B and S6D). TNF receptor-associated factor 6 (TRAF6), a key upstream regulator of TAK1, demonstrated no significant difference during Cis-induced AKI, indicating that CUR may directly target TAK1 rather than upstream TRAF6. Furthermore, the effect of TAK1 in CUR-mediated renal protection was assessed by knocking down *TAK1* in HK-2 cells. *TAK1* was silenced with si*TAK1* in HK-2 cells (Fig. 7C and S6E). As expected, *TAK1* silencing greatly reversed cell damage and apoptosis by Cis-induced, as evidenced by impeding c-PARP and KIM-1 protein levels, along with reduced *KIM-1* and *NGAL* mRNA levels (Fig. 7C–E and S6F-G). Moreover, the inflammatory response was suppressed upon *TAK1* knockdown, as indicated by the decreased *Tnfα, Il6*, and *Il1b* mRNA levels in the si*TAK1* + Cis group compared to the Cis group. Moreover, CUR did not further decrease inflammation in the si*TAK1* + Cis + 5 μM CUR group, unlike the si*TAK1* + Cis group (Fig. 7F–H). Additionally, TAK1 inhibition affected MAPK and NF-κB signalings. Western blotting assays revealed that *TAK1* silencing reduced p-ERK, p-JNK, and p-P38 levels (Fig. 7I and S6H). Similarly, p-p65 and p-IκBα degradation was observed in the *TAK1* silencing group, and TAK1 phosphorylation was also inhibited following *TAK1* knockdown (Fig. 7J and S6I). Consistently, immunofluorescence analysis confirmed that *TAK1* silencing prevented p65 nuclear translocation (Fig. 7K). Consequently, these findings suggest that CUR inhibits TAK1 activation, thereby diminishing Cis-induced AKI.

Discussion

Cis-induced AKI affects 20 %–35 % of chemotherapy patients; however, current management remains palliative rather than mechanistic (Fu et al., 2023). Hydration protocols and electrolyte monitoring fail to address the underlying pathophysiology. Here, we revealed that CUR treatment alleviated Cis-induced nephrotoxicity *in vivo* and *in vitro* (Fig. 8). GO analysis indicated that the protective effect of CUR in Cis-induced AKI was primarily associated with an acute inflammatory response, differing from previous studies that emphasized CUR's antioxidant properties (Jia, et al., 2021). Furthermore, KEGG enrichment analysis identified its unique anti-inflammatory mechanisms *via* MAPK/NF-κB inhibition. Notably, TAK1 was identified as CUR's direct molecular target (binding affinity: –5.73 ± 0.12 kcal/mol), which establishes CUR as the first sesquiterpenoid TAK1 inhibitor, with binding energy suppressing some synthetic TAK1 blockers in the PDBbind database (Wang et al., 2022).

In contrast to existing clinical drugs that are typically administered after cis-induced kidney injury occurs, both preventive and therapeutic administration of CUR have been demonstrated to alleviate Cis-induced AKI (Fig. S7). Preventive administration of CUR provided superior early-phase nephroprotection, possibly through preconditioning renal epithelia against Cis uptake and inducing anti-inflammation pathway in advance. Therapeutic administration of CUR exhibited sustained repair capacity, reversing established tubular damage *via* TAK1-MAPK/NF-κB axis modulation. Moreover, we investigated the effect of CUR on other organs. Notably, CUR showed no toxic effect on other critical organs, including heart, liver, spleen, and lung. These findings highlight the notable advantage of CUR in mitigating Cis-induced AKI, demonstrating its flexibility as both a preventive agent and a therapeutic intervention.

Recently, the inflammatory response has been found to be crucial in AKI (Li et al., 2023). Inflammation is a significant characteristic of renal tubular epithelium damaged by Cis (Fu et al., 2023). Moreover, CUR has potent anti-inflammatory properties across various diseases (Jia et al., 2021; Liu et al., 2024). Our study identified a previously unreported selectivity of CUR in targeting macrophage-mediated inflammation while preserving other immune compartments. Immunohistochemical staining revealed that CUR treatment specifically reduced $F4/80^{+}$-macrophage infiltration without affecting other immune cells: $CD11c^{+}$-dendritic cells, MPO^{+}-neutrophils, $CD4^{+}$-T cells, and $CD19^{+}$-B cells in injured kidneys.

Several signalings, including MAPK, NF-κB, and PI3K/AKT, have been involved in the effects of CUR against various diseases (Xu et al., 2023; Yu et al., 2023b). RNA-seq data revealed that CUR anti-inflammatory impact is primarily related to inhibit MAPK and NF-κB signalings. Kinase activity analysis further revealed that CUR inhibited the enzymatic activities of ERK1/2 (54.83 % ± 7.84 %), JNK1/2 (45.33 ± 5.39 %), P38 (48.77 % ± 6.60 %), and IKKα (50.33 % ± 5.90 %). In AKI models, MAPK and NF-κB pathways are typically activated, playing a key role in modulating kidney inflammation and cellular death in Cis-induced AKI (Fu et al., 2023). MAPK and NF-κB signaling activation is crucial in promoting inflammation in damaged kidneys (Li et al., 2019) . Cis stimulation of renal tissues upregulates ERK1/2, JNK, and P38 phosphorylation, while NF-κB translocates from the cytoplasm to the nucleus, governing inflammatory gene transcription. CUR treatment attenuates Cis-induced ERK1/2, JNK, and P38 phosphorylation while reducing NF-κB and IκBα phosphorylation levels. These findings suggest that CUR protects against Cis nephrotoxicity by modulating the MAPK and NF-κB signalings.

TAK1, a member of the mitogen-activated protein kinase family member, functions as a key regulatory kinase that modulates MAPK and NF-κB signalings, along with inflammatory responses (Sun et al., 2024). TAK1 has been recognized as a crucial serine-threonine kinase essential for regulating immune responses and pro-inflammatory signaling cascades (Wang et al., 2021; Zhao et al., 2024). Recently, TAK1 has been involved in the development of acute damage in the kidney, liver, and brain (Su et al., 2023; Xu et al., 2021; Zhao et al., 2024). Furthermore, TAK1 has been implicated in the modulation of inflammatory effect, oxidative stress, and apoptosis in the renal tubular epithelium (Yang et al., 2024). The TAK1-JNK signaling pathway is activated upon Cis stimulation, leading to apoptosis and inflammation in the tubular epithelium. Consequently, TAK1 deficiency mitigates Cis-induced AKI (Zhou et al., 2020). These findings highlight TAK1 as a key regulator in Cis nephrotoxicity pathogenesis. Notably, TAK1 serves as a critical upstream mediator of NF-κB and MAPK signalings (Wang et al., 2022). Research has demonstrated that certain medications exert anti-inflammatory effects by impeding TAK1, elucidating that TAK1 suppression may offer an effective therapeutic approach for inflammatory diseases (Lan et al., 2022). Therefore, targeting the TAK1-MAPK-NF-κB cascade presents a promising approach to AKI treatment. This study's findings identified TAK1 as CUR's direct molecular target, with a binding affinity of –5.73 ± 0.12 kcal/mol and a pKi of 4.21 ± 0.09 μM. CUR inhibited Cis-induced TAK1 phosphorylation in mouse kidney tissues and cultured renal tubular epithelium, reducing inflammation and dual-inhibition of downstream MAPK and NF-κB cascades. This upstream targeting strategy offers distinct therapeutic advantages: (1) broader pathway coverage than single-kinase inhibitors, (2) enhanced specificity compared to pan-kinase blockers, and (3) reduced compensatory signaling observed with downstream inhibitors. These findings establish a new paradigm in natural product pharmacology by identifying TAK1 as CUR's primary molecular target, providing structural insights for next-generation TAK1 inhibitors development, and validating upstream kinase control as a superior

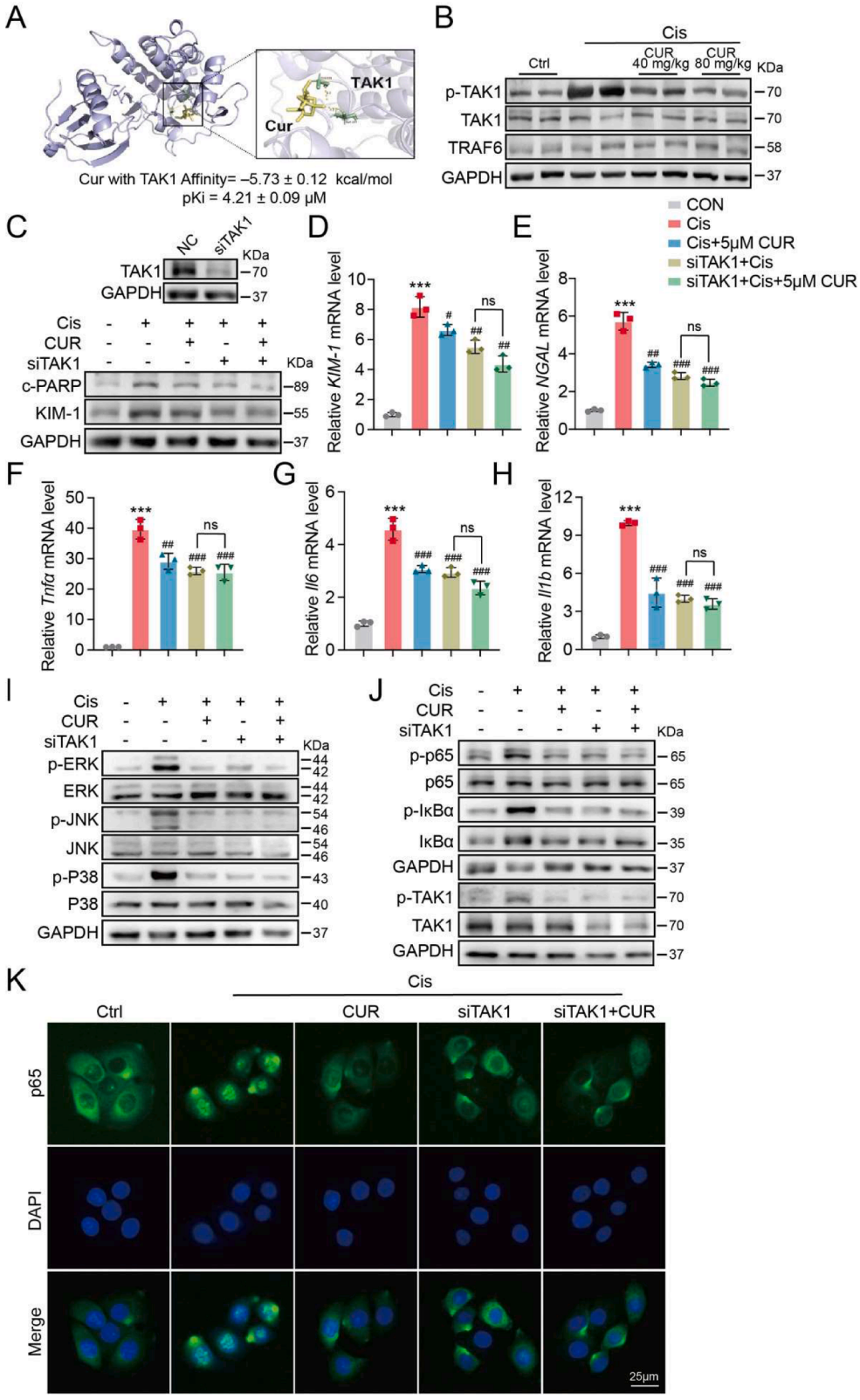

Fig. 7. CUR protected against Cis-induced AKI by inhibiting TAK1. (A) MOD of CUR complexed with TAK1. (B) TAK1, p-TAK1, and TRAF6 protein levels were detected by Western blotting, with GAPDH as the loading control. (C) *TAK1* knockdown efficiency was confirmed through Western blotting assay (upper panel). c-PARP and KIM-1 protein expression levels were examined using Western blotting, GAPDH as the loading control. (D-E) mRNA levels of *KIM-1* and *NGAL* were detected using RT-qPCR, with data normalized to *Gapdh*. (F–H) RT-qPCR measured relative *Tnfα, Il6,* and *Il1b* mRNA levels, and data were normalized to *Gapdh*. (I) Protein levels of ERK, JNK, P38, p-ERK, p-JNK, and p-P38 were analyzed by Western blotting. GAPDH was used as the loading control. (J) The protein levels of p65, IκBα, p-p65, p-IκBα, TAK1, and p-TAK1 were analyzed by Western blotting, with GAPDH as the loading control. (K) Representative images of p65 nuclear translocation were detected using immunofluorescence microscopy. Nuclei were stained with DAPI (scale bar = 25 μm).

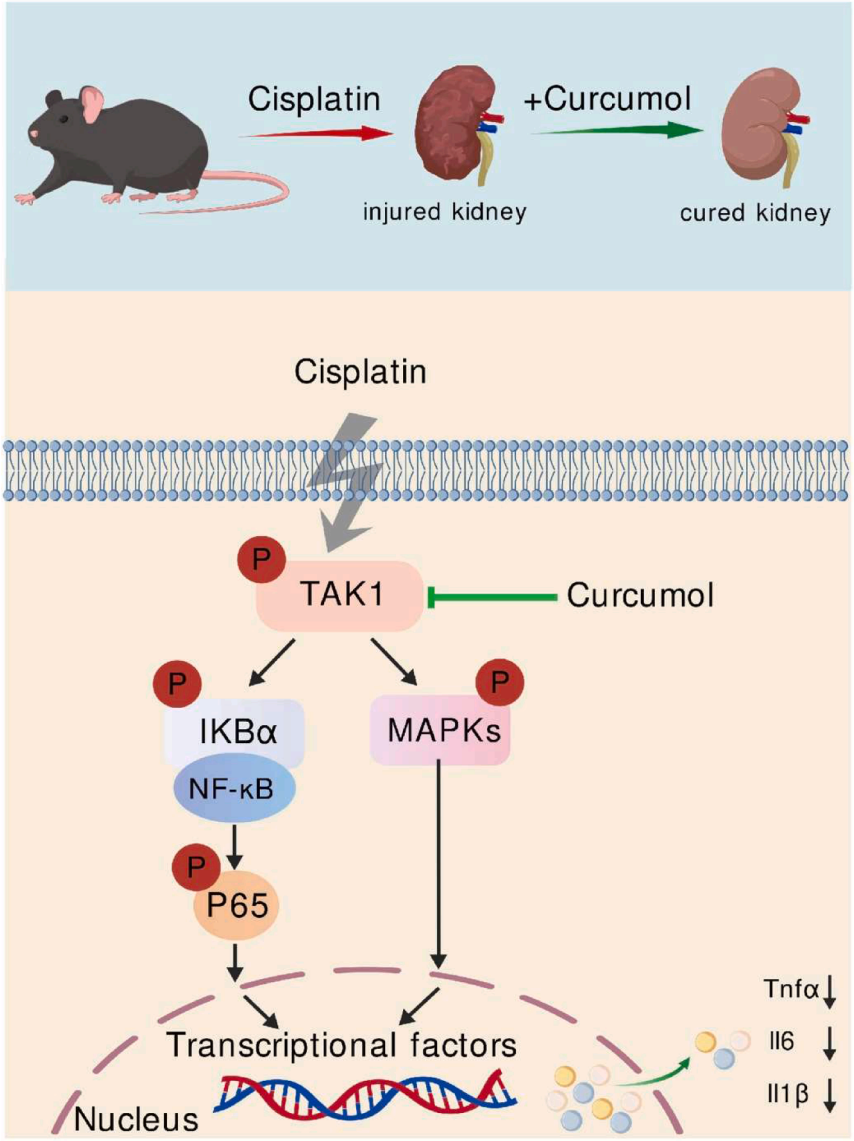

Fig. 8. Schematic diagram of the CUR protective effect against Cis nephrotoxicity. CUR targets TAK1, inhibiting the expression of phosphorylated TAK1, which prevents MAPK and NF-κB signaling activation, thereby decreasing the inflammatory response and protecting against Cis-induced nephrotoxicity. This diagram was created with BioGDP. Com.

therapeutic strategy.

Conclusion

CUR significantly alleviates Cis-induced AKI by suppressing inflammatory responses by suppressing TAK1/MAPK/NF-κB signaling. This study identifies CUR as the first natural compound targeting phosphorylated TAK1 to mitigate Cis nephrotoxicity, introducing a novel therapeutic approach. However, this study has some constraints: First, the mechanistic analysis was primarily conducted in rodent models, necessitating human renal cell-based experiments to confirm translational relevance. Second, the pharmacokinetic profile and long-term safety of CUR remain uncharacterized. Third, potential off-target effects of CUR on other signaling pathways were not thoroughly evaluated. Consequently, future studies should focus on the following areas: 1. Expanding mechanistic scope by integrating human proximal tubular cell lines and organoid models. 2. Optimizing CUR derivatives to enhance bioavailability and reduce toxicity. 3. Exploring synergistic effects with other nephroprotective agents in multi-drug regimens.

Conclusively, CUR is a promising candidate for clinical application, highlighting the need to further explore its therapeutic potential in mitigating chemotherapy-induced organ damage.

CRediT authorship contribution statement

Xuejin Jin: Writing – original draft, Methodology, Investigation, Data curation. **Miao Yuan:** Validation, Methodology, Data curation. **Lingkun Wang:** Investigation, Formal analysis, Data curation. **Huiyan Zha:** Validation, Methodology. **Zhiwei Zheng:** Validation, Software. **Zheng Xu:** Validation, Conceptualization. **Jing Shi:** Formal analysis, Resources. **Guang Liang:** Supervision, Project administration. **Qian Zhou:** Writing – review & editing, Writing – original draft, Funding acquisition, Conceptualization.

Declaration of competing interest

The authors declare that they have no known competing financial interests or personal relationships that could have appeared to influence the work reported in this paper.

Acknowledgement

The study was supported by the General scientific research project of Zhejiang Education Department (Y202456747 for Q.Z.), Operating Expenses of Basic Scientific Research Project of Hangzhou Medical College (KYZD202203 for J.S.), and Key Foundation of Zhejiang Traditional Chinese Medicine Science and Technology Program (GZY-ZJKJ-23056 for J.S.). We thank Ms Xiaoying Xu for providing molecular docking data. We acknowledge the Home for Researchers editorial team (www.home-for-researchers.com) for their language editing services.

Supplementary materials

Supplementary material associated with this article can be found, in the online version, at doi:10.1016/j.phymed.2025.156752.

References

Fang, C.Y., Lou, D.Y., Zhou, L.Q., Wang, J.C., Yang, B., He, Q.J., Wang, J.J., Weng, Q.J., 2021. Natural products: potential treatments for cisplatin-induced nephrotoxicity. Acta Pharmacol. Sin. 42 (12), 1951–1969.

Fu, Y., Xiang, Y., Wang, Y., Liu, Z., Yang, D., Zha, J., Tang, C., Cai, J., Chen, G., Dong, Z., 2023. The STAT1/HMGB1/NF-kappaB pathway in chronic inflammation and kidney injury after cisplatin exposure. Theranostics 13 (9), 2757–2773.

Gao, H., Sun, L., Li, J., Zhou, Q., Xu, H., Ma, X.N., Li, R., Yu, B.Y., Tian, J., 2023. Illumination of hydroxyl radical in kidney injury and high-throughput screening of natural protectants using a fluorescent/photoacoustic probe. Adv. Sci. 10 (33), e2303926.

Jia, S., Guo, P., Lu, J., Huang, X., Deng, L., Jin, Y., Zhao, L., Fan, X., 2021. Curcumol ameliorates lung inflammation and airway remodeling *via* inhibiting the abnormal activation of the wnt/beta-catenin pathway in chronic asthmatic mice. Drug Des. Devel. Ther. 21 (15), 2641–2651.

Kellum, J.A., Romagnani, P., Ashuntantang, G., Ronco, C., Zarbock, A., Anders, H.J., 2021. Acute kidney injury. Nat. Rev. Dis. Primers. 7 (1), 52.

Lan, T., Jiang, S., Zhang, J., Weng, Q., Yu, Y., Li, H., Tian, S., Ding, X., Hu, S., Yang, Y., Wang, W., Wang, L., Luo, D., Xiao, X., Piao, S., Zhu, Q., Rong, X., Guo, J., 2022. Breviscapine alleviates NASH by inhibiting TGF-beta-activated kinase 1-dependent signaling. Hepatology 76 (1), 155–171.

Li, G., Lin, J., Peng, Y., Qin, K., Wen, L., Zhao, T., Feng, Q., 2020. Curcumol may reverse early and advanced liver fibrogenesis through downregulating the uPA/uPAR pathway. PhytOther Res. 34 (6), 1421–1435.

Li, R., Guo, Y., Zhang, Y., Zhang, X., Zhu, L., Yan, T., 2019. Salidroside ameliorates renal interstitial fibrosis by inhibiting the TLR4/NF-kappaB and MAPK signaling pathways. Int. J. Mol. Sci. 20 (5), 1103.

Li, S., Zhang, Y., Lu, R., Lv, X., Lei, Q., Tang, D., Dai, Q., Deng, Z., Liao, X., Tu, S., Yang, H., Xie, Y., Meng, J., Yuan, Q., Qin, J., Pu, J., Peng, Z., Tao, L., 2023. *Peroxiredoxin 1* aggravates acute kidney injury by promoting inflammation through Mincle/Syk/NF-kappaB signaling. Kidney Int. 104 (2), 305–323.

Liu, Y., Wang, W., Di, B., Miao, J., 2024. Curcumol ameliorates neuroinflammation after cerebral ischemia-reperfusion injury *via* affecting microglial polarization and Treg/Th17 balance through Nrf2/HO-1 and NF-kappaB signaling. Cell Death. Discov. 10 (1), 300.

Nie, X., Wu, Z., Shang, J., Zhu, L., Liu, Y., Qi, Y., 2023. Curcumol suppresses endothelial-to-mesenchymal transition *via* inhibiting the AKT/GSK3beta signaling pathway and alleviates pulmonary arterial hypertension in rats. Eur. J. Pharmacol. 943, 175546.

Privratsky, J.R., Ide, S., Chen, Y., Kitai, H., Ren, J., Fradin, H., Lu, X., Souma, T., Crowley, S.D., 2023. A macrophage-endothelial immunoregulatory axis ameliorates septic acute kidney injury. Kidney Int. 103 (3), 514–528.

Shao, Y.F., Tang, B.B., Ding, Y.H., Fang, C.Y., Hong, L., Shao, C.X., Yang, Z.X., Qiu, Y.P., Wang, J.C., Yang, B., Weng, Q.J., Wang, J.J., He, Q.J., 2023. Kaempferide ameliorates cisplatin-induced nephrotoxicity *via* inhibiting oxidative stress and inducing autophagy. Acta Pharmacol. Sin. 44 (7), 1442–1454.

Song, J., Yu, W., Chen, S., Huang, J., Zhou, C., Liang, H., 2024. Remimazolam attenuates inflammation and kidney fibrosis following folic acid injury. Eur. J. Pharmacol. 966, 176342.

Su, W., Gao, W., Zhang, R., Wang, Q., Li, L., Bu, Q., Xu, Z., Liu, Z., Wang, M., Zhu, Y., Wu, G., Zhou, H., Wang, X., Lu, L., 2023. *TAK1* deficiency promotes liver injury and tumorigenesis *via* ferroptosis and macrophage cGAS-STING signalling. JHEP. Rep. 5 (5), 100695.

Sun, T., Wang, F., Li, J., Wei, W., Wang, Y., Tong, Z., Zou, W., 2024. *ISIR* and its human homolog gene *AK131315* strengthen LPS-induced inflammation and acute lung injury by promoting TAK1-dependent NF-kappaB and MAPK signaling. Int. Immunopharmacol. 137, 112510.

Tang, C., Livingston, M.J., Safirstein, R., Dong, Z., 2023. Cisplatin nephrotoxicity: new insights and therapeutic implications. Nat. Rev. Nephrol. 19 (1), 53–72.

Tang, P.M., Nikolic-Paterson, D.J., Lan, H.Y., 2019. Macrophages: versatile players in renal inflammation and fibrosis. Nat. Rev. Nephrol. 15 (3), 144–158.

Wang, B., Yang, L.N., Yang, L.T., Liang, Y., Guo, F., Fu, P., Ma, L., 2024. Fisetin ameliorates fibrotic kidney disease in mice *via* inhibiting ACSL4-mediated tubular ferroptosis. Acta Pharmacol. Sin. 45 (1), 150–165.

Wang, L., Zhang, X., Lin, Z.B., Yang, P.J., Xu, H., Duan, J.L., Ruan, B., Song, P., Liu, J.J., Yue, Z.S., Fang, Z.Q., Hu, H., Liu, Z., Huang, X.L., Yang, L., Tian, S., Tao, K.S., Han, H., Dou, K.F., 2021. Tripartite motif 16 ameliorates nonalcoholic steatohepatitis by promoting the degradation of phospho-TAK1. Cell Metab. 33 (7), 1372–1388.e7.

Wang, S., Li, H., Chen, R., Jiang, X., He, J., Li, C., 2022. *TAK1* confers antibacterial protection through mediating the activation of MAPK and NF-kappaB pathways in shrimp. Fish. Shellfish. Immunol. 123, 248–256.

Wei, W., Rasul, A., Sadiqa, A., Sarfraz, I., Hussain, G., Nageen, B., Liu, X., Watanabe, N., Selamoglu, Z., Ali, M., Li, X., Li, J., 2019. Curcumol: from plant roots to cancer roots. Int. J. Biol. Sci. 15 (8), 1600–1609.

Xu, P., Tao, C., Zhu, Y., Wang, G., Kong, L., Li, W., Li, R., Li, J., Zhang, C., Wang, L., Liu, X., Sun, W., Hu, W., 2021. *TAK1* mediates neuronal pyroptosis in early brain injury after subarachnoid hemorrhage. J. Neuroinflammation. 18 (1), 188.

Xu, W., Ding, J., Kuang, S., Li, B., Sun, T., Zhu, C., Liu, J., Zhu, L., Li, Y., Sheng, W., 2023. Icariin-curcumol promotes docetaxel sensitivity in prostate cancer through modulation of the PI3K-Akt signaling pathway and the Warburg effect. Cancer Cell Int. 23 (1), 190.

Yang, A., Ding, Y., Guo, C., Liu, C., Xiong, Z., Quan, M., Bai, P., Cai, R., Li, B., Li, G., Deng, Y., Wu, C., Sun, Y., 2024. *PARVB* deficiency alleviates cisplatin-induced tubular injury by inhibiting TAK1 signaling. Cell Mol. Life Sci. 81 (1), 385.

Yao, W., Chen, Y., Li, Z., Ji, J., You, A., Jin, S., Ma, Y., Zhao, Y., Wang, J., Qu, L., Wang, H., Xiang, C., Wang, S., Liu, G., Bai, F., Yang, L., 2022. Single cell RNA sequencing identifies a unique inflammatory macrophage subset as a druggable target for alleviating acute kidney injury. Adv. Sci. 9 (12), e2103675.

Yu, B., Jin, L., Yao, X., Zhang, Y., Zhang, G., Wang, F., Su, X., Fang, Q., Xiao, L., Yang, Y., Jiang, L.H., Chen, J., Yang, W., Lin, W., Han, F., 2023. *TRPM2* protects against cisplatin-induced acute kidney injury and mitochondrial dysfunction *via* modulating autophagy. Theranostics 13 (13), 4356–4375.

Yu, Y.H., Zhang, H.J., Yang, F., Xu, L., Liu, H., 2023b. Curcumol, a major terpenoid from *curcumae rhizoma*, attenuates human uterine leiomyoma cell development *via* the p38MAPK/NF-kappaB pathway. J. Ethnopharmacol. 310, 116311.

Zhao, Y., Fan, S., Zhu, H., Zhao, Q., Fang, Z., Xu, D., Lin, W., Lin, L., Hu, X., Wu, G., Min, J., Liang, G., 2024. Podocyte *OTUD5* alleviates diabetic kidney disease through deubiquitinating TAK1 and reducing podocyte inflammation and injury. Nat. Commun. 15 (1), 5441.

Zhou, J., An, C., Jin, X., Hu, Z., Safirstein, R.L., Wang, Y., 2020. *TAK1* deficiency attenuates cisplatin-induced acute kidney injury. Am. J. Physiol. Renal. Physiol. 318 (1), F209–F215.